Kinetics of the Anaerobic Reaction of *para*-Substituted Phenols with Nitrogen Dioxide

JAEL REYES,[1] EDUARDO LISSI,[1] CAMILO LÓPEZ-ALARCÓN,[2] MARÍA A. RUBIO[1,3]

[1]*Facultad de Química y Biología, Universidad de Santiago de Chile, Santiago,* 8320000, *Chile*

[2]*Facultad de Química, Pontificia Universidad Católica de Chile,* PUC, *Santiago, Chile*

[3]CEDENNA, *Universidad de Santiago de Chile, Santiago,* 8320000, *Chile*

Received 18 July 2016; revised 3 October 2016; accepted 4 October 2016

DOI 10.1002/kin.21054
Published online in Wiley Online Library (wileyonlinelibrary.com).

ABSTRACT: *para*-Substituted phenols in aqueous solution under anaerobic conditions readily react with nitrogen dioxide ($NO_2^\bullet$) over a wide range of experimental conditions. The rate and rate law of the process were dependent on phenol concentration and solution pH. The kinetic order in phenol changed from one (low concentration) to zero (high concentration), a result attributable to total $NO_2^\bullet$ capture. Initial consumption rate (r_0) of phenols versus pH plots showed parabolic behavior with a minimum rate at pH ca. 5. On the other hand, the maximum rate took place at high pH (pH>10) and involved the protonated phenols. The reaction rate of para-substituted phenols with $NO_2^\bullet$ correlated with the bond dissociation energy and with Hammett's parameter. Based on such results and also supported by analysis of products carried out by HPLC-MS/MS, our data conclusively show that, in spite of the fast acid–base interchanges of phenols and the interconversion of the different nitrogen oxides, the mechanisms of phenols nitration mediated by $NO_2^\bullet$ or HONO are clearly different. © 2016 Wiley Periodicals, Inc. Int J Chem Kinet 1–9, 2016

INTRODUCTION

Nitrogen oxides constitute a family of free radicals ($NO^\bullet$, $NO_2^\bullet$, $NO_3^\bullet$) characterized by a rich chemistry with relevance in a variety of fields, ranging from air chemistry to biological processes [1–5]. In particular, the chemistry of the reactions involving $NO_2^\bullet$ has attracted the attention of researchers, since such reactive species are capable of reacting with a wide range of organic compounds. Among the compounds able to neutralize $NO_2^\bullet$, phenols appear as one of the most important substrates [6–11]. The reaction between phenols and $NO_2^\bullet$ takes place due to the relatively weak strength of the oxygen–hydrogen bond in these compounds, allowing their participation in hydrogen transfer processes, such as that depicted in Reaction (R1) [12].

Correspondence to: M. A. Rubio; e-mail: maria.rubio@usach.cl.

$$Ph - O - H + NO_2^\bullet \rightarrow Ph - O^\bullet + HONO \quad (R1)$$

While the reaction of phenols with $NO_2^\bullet$ is not relevant in the gas phase, in aqueous solutions is particularly favored by the inclusion of electron-donating groups in the para position of such derivatives [10]. This is directly associated with the capacity of phenols to stabilize the secondary free radicals (phenoxyl radicals) generated as a consequence of the hydrogen abstraction triggered by $NO_2^\bullet$ [10]. Conversely, at high pHs (higher of phenols p*K*a), the energetically favorable oxidation of phenolates to phenoxyl radicals is promoted by the concomitant reduction of $NO_2^\bullet$ to nitrite in a plain electron transfer process (Reaction (R2):

$$Ph - O^- + NO_2^\bullet \rightarrow Ph - O^\bullet + NO_2^- \qquad (R2)$$

The rate constant of Reaction (R1) increases when the strength of the H–O bond in the phenols decreases [10], whereas the rate constant of Reaction (R2) is determined by the oxidation potential of the phenolate ion. In para-substituted phenols, the rate of the electron transfer to $NO_2^\bullet$ will be then determined by the value of the sigma (σ^+) parameter of the substituent group.

Reactions (R1) and (R2) are simple processes that represent elementary steps and follow bimolecular kinetics whose rate constants have been previously determined by time-resolved pulse radiolysis [13]. However, steady-state measurements of these reactions are difficult to interpret. This is mainly due to the fast interchange among reactive nitrogen species such as $NO^\bullet$, $NO_2^\bullet$, NO_2^-, $NO_3^\bullet$, HONO, N_2O_3, and N_2O_4 [14]. Additionally, the descriptions of such reactions are complex since each reactive species is distributed between the aqueous solution and the gas phase [4,14]. To get more insight into the influence of the chemical structure of the phenol on the kinetics of the above-mentioned reactions, in the present work we studied the consumption of para-substituted phenols, bearing electron donor and acceptor groups, triggered by $NO_2^\bullet$, and the results were compared with those previously reported employing HONO as a reactant. For this purpose, solutions containing phenols were kept at known experimental conditions (concentration, ionic strength, and pH) and bubbled with a continuous flux of a gas mixture of nitrogen and $NO_2^\bullet$ [14] or exposed to HONO. In addition, and taking into account the importance of cinnamic acid derivatives in the antioxidant field, we compared results obtained employing para-substituted phenols with coumaric, ferulic, and sinapic acids.

EXPERIMENTAL

Reagents

Trolox (6-hydroxy-2,5,7,8-tetramethylchromane-2-carboxylic acid), PGR (pyrogallol red), ABTS (2,2′-azino-bis(3-ethylbenzothiazoline-6-sulfonic acid)diammonium salt), *N*-(1-naphthyl) etilendiamine, sulfanilamide, phosphoric acid, phenol, *para*-hydroxyphenol, *para*-methoxyphenol, *para*-nitrophenol, coumaric acid (*trans*-4-hydroxycinnamic acid), ferulic acid (4-hydroxy-3-methoxycinnamic acid), and sinapic acid (3,5-dimethoxy-4-hydroxycinnamic acid) were purchased from Sigma Aldrich (St. Louis, MO). Powdered metallic cooper, sodium nitrite (primary standard), nitric acid, hydrochloric acid, phosphorous acid, and sodium chloride were purchased from Merck (Darmstadt, Germany). Nitrogen was purchased from Linde Gas (Santiago, Chile).

$NO_2^\bullet$ Generation

$NO_2^\bullet$ was produced by the oxidation of metallic Cu^0 induced by HNO_3, according to Reaction (R3):

$$Cu^0_{(s)} + 4\,HNO_3 \rightarrow (Cu\,II) + 2\,NO_3^- + 2\,NO_2^\bullet + 2\,H_2O \qquad (R3)$$

To this purpose, 10 mg of powdered metallic Cu^0 was suspended in 20 mL of water, and 30 mL of concentrated HNO_3 was added. The produced $NO_2^\bullet$ was transferred to the reactor (volume ca. 500 mL) by a nitrogen stream (Fig. 1). The total flow of gases was kept at ca. 45 mL/min. The $NO_2^\bullet$ reaching the reacting cell was

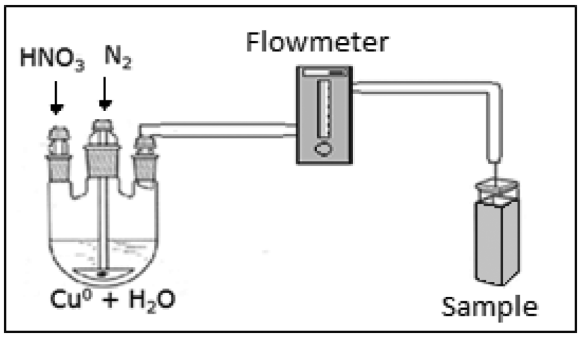

Figure 1 Scheme of the system employed to generate $NO_2^\bullet$. Concentrated HNO_3 was added to a suspension of metallic Cu^0 in water. The suspension was exposed to a constant flux of nitrogen, employed as carrier gas, adjusted at a flux of 45 mL/min. A mixture of N_2 and $NO_2^\bullet$ was continuously bubbled into a reaction cell containing the sample.

titrated as nitrite-employing Griess' assay. To this aim, 3.0 mg of *N*-(1-naphthyl) etilendiamine was solubilized in 3 mL of bidistilled water (named solution A). A second solution (named solution B, Griess' reagent) was prepared by solubilizing 30 mg of sulfanilamide in a mixture of 2.8 mL of water and 0.2 mL of phosphoric acid. For nitrite quantification, equal volumes of solutions A and B were added to each sample. After 30 min incubation at 4ºC in the dark, the absorbance of the sample was measured at 543 nm and the total nitrite (NO_2^- + HONO) concentration was determined from a calibration plot employing $NaNO_2$ as primary standard.

Reaction of Phenols with $NO_2^\bullet$ and HONO: Kinetics of Phenol Consumption and Formation of Oxidized Products

To follow the kinetics of the reaction between para-substituted phenols or cinnamic acid derivatives and $NO_2^\bullet$, aqueous solutions of phenols were bubbled with a nitrogen flow enriched in $NO_2^\bullet$. At different incubation times, aliquots were taken and analyzed by high-performance liquid chromatography (HPLC) coupled to a diode array detector (DAD). The HPLC–DAD system (Agilent 1200 series) employed a C-18 column, and the mobile phase (isocratic) was a mixture of potassium phosphate (10 mM, pH 2.6) with acetonitrile in an 80/20 V/V ratio. As HONO is generated as a product of the reaction (Reaction (R2), the consumption of phenols elicited by this reactive species was also measured. Thus, solutions containing para-substituted phenols (50–100 μM) and nitrite (2–200 μM) were incubated at pH 2 with 17 mM NaCl solution and analyzed by the same HPLC–DAD system.

Formation of oxidized products was studied by HPLC with mass detection (MS/MS). Aliquots of working solutions were analyzed employing an Eksigent model ultra LC 100-XL with a Triple Quad 4500 detector. An Inersil ODS-4 C18, 3 μm (particle size) 2.1 × 100 mm column size, GL Science (Tokyo, Japan) was kept thermostated at 40°C. Formic acid 0.1% in water and acetonitrile was used as a mobile phase, and mass detection (ESI-MS/MS) was carried out employing a negative ionization mode.

RESULTS AND DISCUSSION

Rate of $NO_2^\bullet$ Introduction into the Reaction Cell

Taking advantage of the oxidizing ability of $NO_2^\bullet$ and the spectroscopic properties of PGR and ABTS cation radical ($ABTS^{\bullet+}$), the $NO_2^\bullet$-mediated consumption of the former and the production of the latter were employed to assess the rate of $NO_2^\bullet$ introduction into the reaction cell. In addition, the consumption of Trolox, a hydrosoluble vitamin E analogue, was also determined.

In aqueous solutions (pH 7.4), PGR presents an absorption spectrum with an absorption characterized by a band with a maximum in absorbance at 540 nm. The intensity of this band decreases when PGR is oxidized (forming a quinone as single product) by reactive species such as $NO_2^\bullet$, hypochlorite, peroxynitrite, and peroxyl radicals [15,16]. In the presence of $NO_2^\bullet$, it was observed a decrease of the absorbance of PGR at 540 nm, together with the formation of a new band with a maximum near 380 nm (Fig. 2). From kinetic data (such as that shown in Fig. 2), we determined the initial consumption rate of PGR (r_0) in a wide range of initial concentrations at a fixed flux (45 mL/min) of the (N_2 + $NO_2^\bullet$) gas mixture. Figure 3 shows the dependence of r_0 values with the initial concentration of PGR. As it is shown, at PGR concentration lower than 30 μM, r_0 was proportional to the PGR concentration. However, above this concentration, r_0 values reached a plateau at 0.8 μM/min (Fig. 3). This behavior implies first- and zero-order kinetics in PGR, at low and high PGR concentrations, respectively. Moreover, the presence of a plateau indicates that all the incoming $NO_2^\bullet$ molecules are trapped by PGR. If it is assumed that one PGR molecule removes two $NO_2^\bullet$ radicals; an input rate of $NO_2^\bullet$ ca. 1.6 μM/min can be estimated.

ABTS readily reacts with $NO_2^\bullet$ generating the cationic free radical ($ABTS^{\bullet+}$) as a principal product. In the presence of $NO_2^\bullet$, the intensity of the UV–visible band of ABTS at 340 nm decreases, generating four main bands in the visible region at 413, 646, 734, and 820 nm and an isosbestic point at 380 nm (Fig. 4). The intensity of the band at 734 nm has been commonly employed to assess $ABTS^{\bullet+}$ concentration ($\varepsilon_{734} = 1.3 \times 10^4\ M^{-1}\ cm^{-1}$) [17]. Assuming a total removal of $NO_2^\bullet$ from the incoming gas flow, and that one molecule of ABTS reacts with one molecule of $NO_2^\bullet$, the rate of $ABTS^{\bullet+}$ formation implies that ca. 1.6 μM/min of $NO_2^\bullet$ is introduced into the reaction cell.

Trolox is a water-soluble phenol that readily reacts with free radicals (X·) removing two free radicals per each molecule of Trolox, according to Reaction (R4).

$$2X^\bullet + \text{Trolox} \rightarrow \text{products} \qquad \text{(R4)}$$

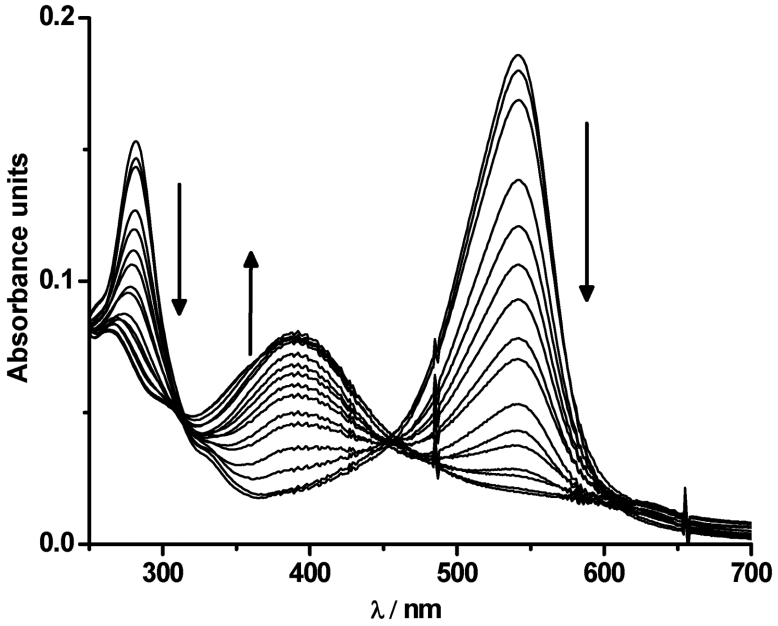

Figure 2 Bleaching of PGR (5 μM) induced by $NO_2^{\bullet}$ after 0 and 20 min of reaction in phosphate buffer (75 mM) at pH 7.4 and 25°C. Arrows indicate the decrease or increase of the corresponding band intensity.

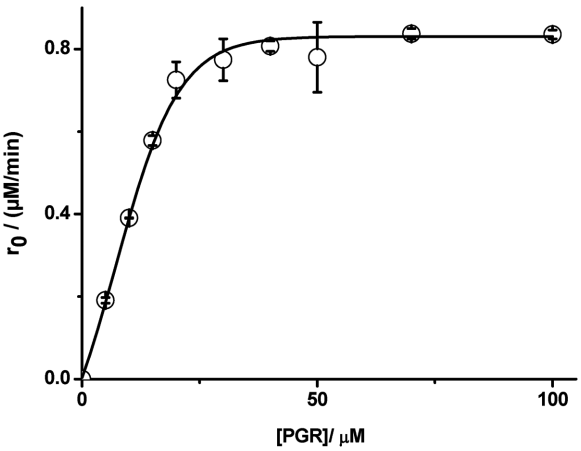

Figure 3 Dependence of the initial consumption rate (r_0) of PGR elicited by $NO_2^{\bullet}$ addition. The solution was incubated in phosphate buffer (75 mM at pH 7.4) and 25°C. r_0 values were determined from the slope, extrapolated at zero reaction time.

At high concentrations, Trolox traps all the free radicals introduced into the system. Thus, during its exposure to the gas mixture, all the $NO_2^{\bullet}$ can react forming quantitatively nitrite as one of the main reaction products (at pH 7.4). The titrating of nitrite by Griess assay showed that $NO_2^{\bullet}$ was introduced to the system at a rate of 1.7 μM/min (Fig. 5). Remarkably, this value is close to those determined from the consumption of PGR or the formation of $ABTS^{\bullet+}$ radical cation.

Role of HONO in the Reaction of $NO_2^{\bullet}$ with Para-Substituted Phenols

Irrespective of the initial nitrogen bearing compound ($NO_2^{\bullet}$ or HONO), a large number of substances ($NO^{\bullet}$, $NO_2^{\bullet}$, HONO, NO_2^-, N_2O_3, N_2O_4) are present along the reaction and can contribute to the phenol modification and consumption [18]. To assess this point, and taking into account the formation of nitrite as product of the reaction between $NO_2^{\bullet}$ and phenols, we measured the initial consumption rate of *para*-methoxyphenol following HONO or $NO_2^{\bullet}$ anaerobic addition over a wide range of pH (2–12). Also, we compared the relative rate of reaction for the family of cinnamic acid derivatives composed by coumaric, ferulic, and sinapic acids and the effect of electron donor and electron acceptor groups in *para* position.

Reaction Rate of Para-Methoxyphenol with $NO_2^{\bullet}$: Effect of pH. Figure 6 presents the dependence of the initial consumption rate of *para*-methoxyphenol, promoted by $NO_2^{\bullet}$, with the pH of the medium. This profile can be explained by the formation of nitrite, and its conjugated acid (p*K*a = 3.14), and the presence of the *para*-methoxyphenol and its phenolate (p*K*a = 10.2). In this context, the left branch of the plot would imply that HONO is more reactive than NO_2^- toward the protonated phenol. Similarly the right branch would indicate that phenolates are more reactive than the protonated compounds.

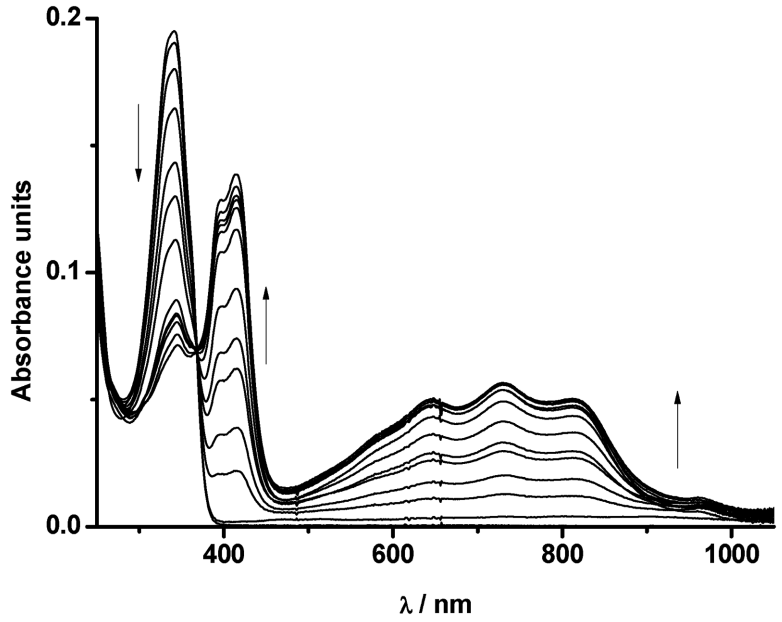

Figure 4 ABTS (20 μM) consumption and $ABTS^{\bullet+}$ cation formation induced by $NO_2^{\bullet}$ between 0 and 30 min of reaction in phosphate buffer (75 mM) at pH 7.4 and 25°C. Arrows indicate the decrease or increase of the band intensity.

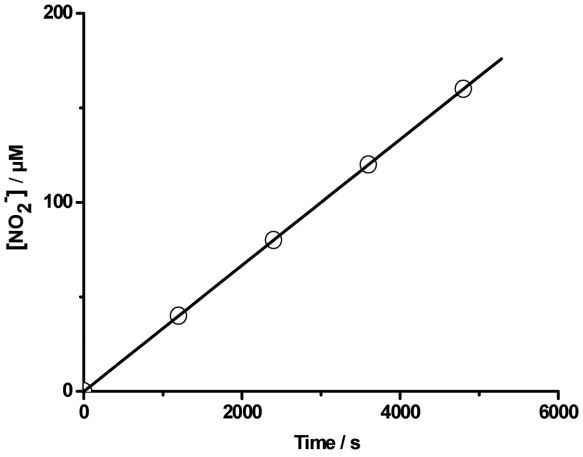

Figure 5 Concentration of $NO_2^{\bullet}$ generated by the Cu^0/HNO_3 system. $NO_2^{\bullet}$ concentration was determined by the formation of nitrite ions (NO_2^-) during the reaction of $NO_2^{\bullet}$ with an excess of Trolox. NO_2^- was determined by the Griess methodol. Trolox solutions were incubated in phosphate buffer (75 mM, pH 7.4 and 25°C) and bubbled with the gas mixture comprising N_2 and $NO_2^{\bullet}$.

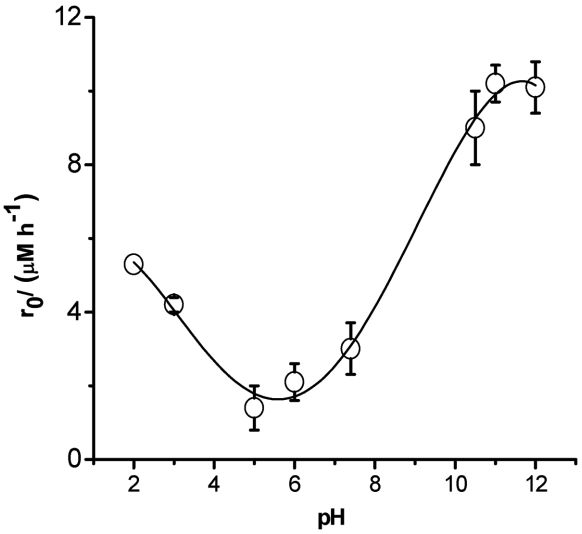

Figure 6 Dependence of the initial consumption rate (r_0) of *para*-methoxyphenol (10 μM) induced by $NO_2^{\bullet}$ at different pHs.

The faster rate of the phenol/$NO_2^{\bullet}$ interaction takes place at pH >10 and hence must involve the deprotonated HONO and *para*-methoxyphenol and can be represented by Reaction (R2). It is interesting to note that $NO_2^{\bullet}$ to NO_2^- reduction increases its water solubility, favoring the nitration of the phenols.

At low pH (<5), the protonated phenol is removed faster by HONO (excess) than by the nitrite anion. The process can take place through a complex mechanism (such as proton-coupled electron transfer) [19] and can be represented by

$$HONO + PhOH \rightarrow NO^{\bullet} + PhO^{\bullet} + H_2O \quad (R5)$$

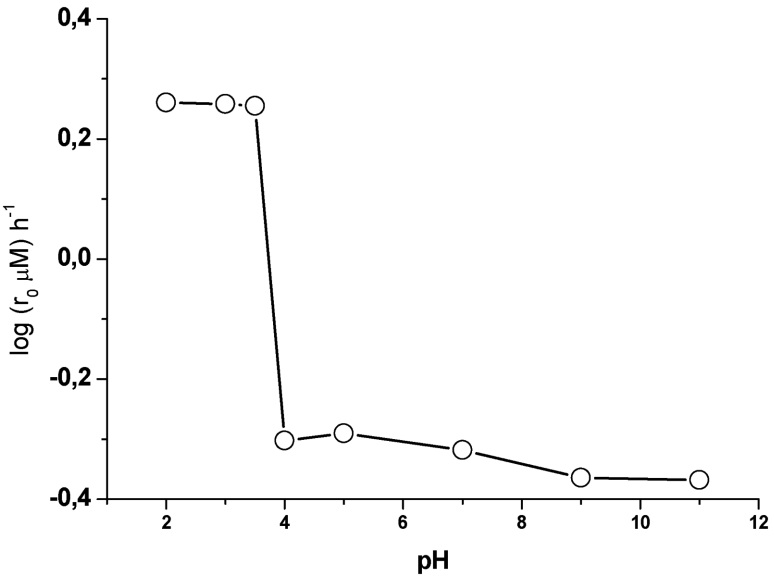

Figure 7 Dependence of the log of initial consumption rate (log r_0) of *para*-methoxyphenol, elicited by HONO, at different pHs. Measurements were carried out under continuous N_2 bubbling.

Figure 6 shows that more than one mechanism is operative in the reaction of phenols with $NO_2^\bullet$. Furthermore, the difference in the profiles obtained employing $NO_2^\bullet$ (Fig. 6) and HONO (Fig. 7) shows that, in spite of the fast conversions between different forms of nitrogen oxides, the mechanism of $NO_2^\bullet$ and HONO promoting nitration of phenols is clearly different. These differences remain even when HONO reaction is carried out under continuous nitrogen bubbling (anaerobic condition).

The occurrence of different mechanisms at different pHs is a frequent feature of $NO_2^\bullet$ + HONO reactions [18,20,21] The data of phenol reaction with HONO represented in Fig. 7 show that the fastest rate takes place at low pH according to Reaction (R5) [14,22]. Conversely, the slowest reaction takes place at pH ≈11 involving nitrite and phenolate anions as reactants.

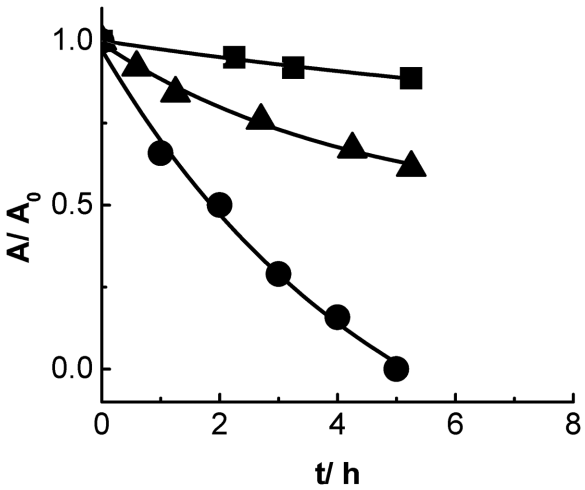

Figure 8 Kinetics profiles of phenol consumption by $NO_2^\bullet$ addition. Solutions of phenol (■), *para*-hydroxyphenol (▲), and *para*-methoxyphenol (⊙) at 10 μM were incubated under a NO_2 flow (1.8 μM/min) at pH 7.4 and 25°C.

Consumption rate of Cinnamic Acid Derivatives: Dependence of the Phenol Concentration and their Characteristics

Figure 8 shows typical results of the kinetic profiles of phenol consumption elicited by $NO_2^\bullet$. From these kinds of data, initial consumption rates (r_0) were determined and plotted as the function of phenol concentration (Fig. 9). As this figure shows, at low concentration, the rate depends of the compound considered and its concentration. However, at high concentrations, r_0 of the studied compounds (except coumaric acid) reached a plateau at similar values ≈0.9 and 0.4 μM/min for *para*-substituted phenols (Fig. 9A) and cinnamic acids (Fig. 9B), respectively. These plateaus were independent of the compound reactivity, suggesting total trapping of the $NO_2^\bullet$ present in the gas flow. This indicates that secondary reactions barely contribute to the total rate of the process, at least for monophenols [23]. It is interesting to note that the comparison of the value in the plateau with the rate of incorporation of $NO_2^\bullet$ (≈1.7 μM/min) leads to the conclusion that nearly two

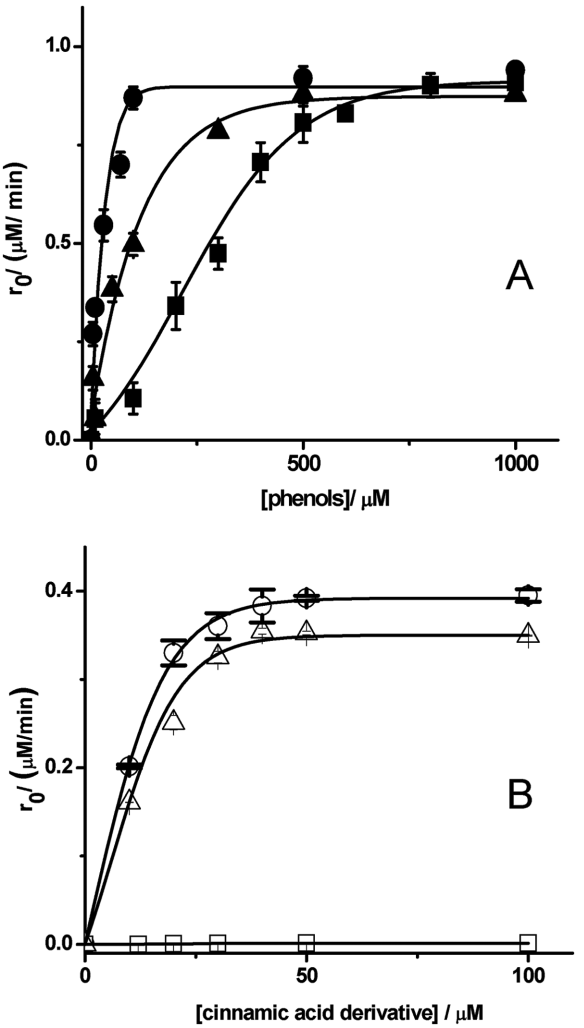

Figure 9 Dependence of the initial consumption rate (r_0) of phenolic compounds (graphic A) and cinnamic acid derivatives (graphic B) elicited by $NO_2^\bullet$ with its initial concentration. Solutions of phenol (■), *para*-hydroxyphenol (▲), *para*-methoxyphenol (⊙), sinapic acid (○), ferulic acid (△), and coumaric acid (□) were incubated in phosphate buffer (75 mM, pH 7.4, at 25°C) and bubbled with a gas mixture of N_2 and $NO_2^\bullet$ at 1.8 μM/min.

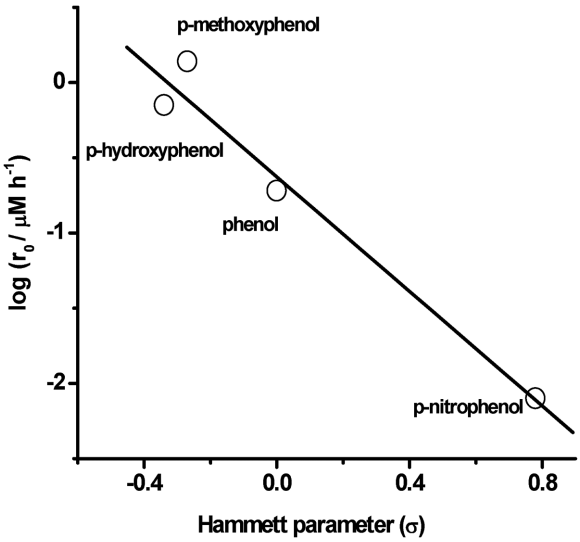

Figure 10 Dependence of log of the initial consumption rate (log r_0) of para-substituted phenol derivatives with their Hammett`s sigma parameters (σ). Solutions were incubated at 25°C at pH 5.0 in the presence of a $NO_2^\bullet$ flow ($R = 0.997$; $p = 0.00276$).

$NO_2^\bullet$ molecules were consumed by each reacted phenol. In the cases of sinapic and ferulic acids, near four molecules of $NO_2^\bullet$ react with each derivative. However, at low concentrations, the relative reactivity of cinnamic acid derivatives toward $NO_2^\bullet$ was similar to that reported for their reactivity toward peroxyl radicals [23]. This is in agreement with the fact that the bond dissociation energy (BDE) of the H–O bond follows the trend:

Sinapic acid (76.9 kcal/mol) < ferulic acid (81.9 kcal/mol) < coumaric acid (84.3 kcal/mol) making the weakest bond in sinapic acid nearly 50 times more labile than that of coumaric acid. However, it must be taken into account that both, $NO_2^\bullet$ and phenols, are, particularly at low pHs, distributed between the gaseous and liquid phases of the reactor (Fig. 1), precluding a sound quantitative evaluation of the aqueous phase rate constants [4,14].

The other critical parameter controlling the rate of the reaction between a para-substituted phenol and $NO_2^\bullet$ is the electrophilicity of the substituent group. This factor can be quantified by the value of Hammett's parameter (σ). This effect is clearly evidenced in the data depicted in Fig. 10, which show a dependence of the phenol consumption rate (r_0), induced by $NO_2^\bullet$, with the charge density in the aromatic ring. The negative slope (–2.0) emphasizes the electroaffinity of the process. Other values reported in closely related works were –1.23 for HONO [14] and –3 for NO_2^- [24], in which the largest slope corresponds to a simple electron transfer processes.

The rate of the reaction of para-substituted phenols with $NO_2^\bullet$ correlated with the BDE: *para*-methoxyphenol (81.3 kcal/mol), *para*-hydroxyphenol (81.7 kcal/mol), phenol (87.5 kcal/mol), and *para*-nitrophenol (91.7 kcal/mol) [25] and with Hammett's parameter (σ): *para*-methoxyphenol (–0.3), *para*-hydroxyphenol (–0.4), phenol (0.0), and *para*-nitrophenol (0.8). This emphasizes the relationship between BDE and charge density at the aromatic ring ($R = 0.951$; $p = 0.048$).

Products of the Reaction between Phenols and $NO_2^\bullet$

Phenol. $NO_2^\bullet$ and, in a smaller degree phenols, are distributed among the gas and liquid phases present in the reactor. This mimic what take place in the atmosphere where they are distributed between the gas phase an wet particles and/or micrometeors [26,27]. This precludes a quantitative evaluation of the kinetics of the chemical processes. In spite of that, HPLC coupled to MS/MS can provide an insight of the main products produced in the nitration/oxidation of the phenols at different stages of the reaction. In fact, the MS/MS characterization of the obtained product of the reaction of phenol toward $NO_2^\bullet$ gave a molecular ion of 139.1, corresponding to a mono-nitrophenol derivative. The formation of such product can be attributed to a hydrogen atom transfer from the phenol group to the $NO_2^\bullet$ (Reaction (R1) [7], followed by a rearrangement and reaction with another $NO_2^\bullet$ molecule. This initial step can involve $NO_2^\bullet$ or HONO [18] but cannot be due to a NO–phenol adduct (molecular mass 123).

para-*Methoxyphenol***.** The main molecular product presents a molecular mass of 168.8, which can be attributed to 4-methoxy-2-nitrophenol. The mechanism underlying the formation of this product is similar to that above discussed for phenol.

Sinapic acid. The main reaction product includes three nitro-groups (molecular mass 358.7). It is proposed that, following an initial hydrogen abstraction from the phenol group, it takes place an addition to the lateral aliphatic chain, rendering 3,4-dihydroxy-5-methoxy-3-methyl,2-nitrophenyl,2,3-dinitropropanoic acid as a main product. This reaction path emphasizes the capacity of $NO_2^\bullet$ to add to activated double bonds [6,28].

CONCLUSIONS

para-Substituted phenols readily react with $NO_2^\bullet$ over a wide range of experimental conditions. The rate and rate law of the process depend on the phenol concentration and the pH of the solution. In particular, the main first-generation products and the pH dependence of the reaction of $NO_2^\bullet$ with *para*-substituted phenols imply that the mechanism of the process differs for HONO and $NO_2^\bullet$.

The rate of the process at the fixed phenol concentration (10 μM) shows a parabolic-like dependence with the pH, with a minimum at pH ca. 5. This indicates that low pH HONO favors the reaction, whereas at high pH deprotonation of phenols disfavors it.

The rate of the reaction of para-substituted phenols with $NO_2^\bullet$ correlated with their BDE and Hammett's σ parameter

This work was supported by FONDECYT (grants no 1141142), DICYT (Projects Numbers 091541LG and 041501RC) and Centers of Excellence with Basal/CONICYT financing, Grant FB0807, CEDENNA.

BIBLIOGRAPHY

1. Wardman, P. J Radioanal Nucl Chem 1998, 232, 23–27.
2. Augusto, O.; Bonini, M. G.; Amanso, A. M.; Linares, E.; Santos, C. C. X.; De Menezes, S. I. Free Radical Biol Med 2002, 32, 841–859.
3. Vione, D.; Maurino, V.; Minero, C.; Borghes, i. D.; Lucchiari, M.; Pelizzetti, E. Environ Sci Technol 2003, 20, 4635–4641.
4. Amman, M.; Roessler, E.; Strekowski, R.; George, C. Phys Chem Chem Phys 2003, 7, 2513–2518.
5. Stemmler, K.; Amman, M.; Donders, C.; Kleffmann, J.; George, C. Nature 2006, 440, 195–198.
6. Cooney, R. J.; Ross, P. D. J Agri Food Chem 1987, 35, 789–796.
7. Zhouen, Z.; Side, Y.; Weizhen, L.; Wenfing, W.; Niayun, L. Free Radical Res 1998, 29, 33–36.
8. Hartshorn, M. P. Acta Chem Scand 1998, 52, 2–10.
9. Kumar, V.; Kalite, A.; Mondal, B. M. Dalton Trans 2013, 42, 16264–16267.
10. Shenghur, A.; Weber, K. H.; Nguyen, N. D.; Sontising, W.; Fu-Ming, T. J Phys Chem A 2014, 118(46), 11002–11014.
11. Yuan, B.; Liggio, J.; Wentzell, J.; Li, S-M.; Stark, H.; Robert, J. M.; Gilman, J.; Lerner, B.; Warneke, C.; Li, R.; Leithead, A.; Osthoff, H. D.; Wild, R.; Brown, S., de Gouw, J. A. Atmos Chem Phys 2016, 16, 2139–2153.
12. Fukuto, J. M.; Carrington, S. J.; Tantillo, D. J.; Harrison, J. G.; Ignarro, L. J.; Freeman, B. A.; Chen, A.; Wink, D. A. Chem Res Toxicol 2012, 25, 769–793.
13. Alfassi, Z. B.; Huie, R. E.; Neta, P. J Phys Chem 1986, 90, 4156–4158.
14. Rubio, M. A.; Lissi, E.; Olivera, N.; Reyes, J. L.; López-Alarcon, C. Int J Chem Kinet 2014, 46,143–150.
15. Atala, E.; Velasquez, G.; Vergara, C.; Mardones, C.; Reyes, J.; Tapia, R. A.; Quina, F.; Mendes, M.; Speisky, H.; Lissi, E. J Phys Chem B 2013, 117, 4870–4879.
16. Hugo, E.; Reyes, J.; Montupil, E.; Bridi, R.; Lissi, E.; Denicola, M.; Rubio, M. A.; Lopez-Alarcon, C. Molecules 2015, 20, 10582–10593.
17. Henriquez, A.; Lissi, E. Bol Soc Chil Quím 2002, 47, 563–566.
18. Vione, D.; Belmondo, S.; Carnino, L. Environ Chem Lett 2004, 2, 135–139.
19. Koper, M. T. Chem Sci 2013, 4, 2710–2723.
20. Elias, G.; Mincher, B. J.; Mezyk, S. P.; Cullen, T. D.; Martin, L. R. Environ Chem 2010, 7, 183–189.

21. Kroflič, A.; Grilc M.; Grgić I. Environ Sci Technol 2015, 49(15), 9150–9158.
22. Beake, B.; Constantine, J. L.; Moodie, R. J Chem Soc, Perkin Trans 1994, 2, 335–340.
23. Pino, E.; Campos, A. M.; Lopez-Alarcon, C.; Aspee, A.; Lissi, E. J Phys Org Chem 2006, 19. 759–764.
24. Alfassi, Z. B., Huie, R. E., Neta, P. J Phys Chem 1986, 90, 4156–4159.
25. Chandra A. K., Uchimaru T. Int J Mol Sci 2002, 3, 407–422.
26. Rubio, M. A.; Lissi, E.; Villena-Tapia, G. Atmos Environ 2008, 42, 7651–7656.
27. Rubio, M. A.; Lissi, E.; Herrera, N.; Pérez, V.; Fuentes, N. Chemosphere 2012, 86, 1035–1039.
28. Encinas, M. V.; Norambuena, E.; Lissi, E. Macromolecules 1998, 31, 5171–5174.